International Communications in Heat and Mass Transfer 49 (2013) 41–48

Contents lists available at ScienceDirect

International Communications in Heat and Mass Transfer

journal homepage: www.elsevier.com/locate/ichmt

An enhancement of the back region forced convection heat transfer rates of a reciprocating curved channel with a rib by the ALE method ☆

Wu-Shung Fu *, Yu-Chih Lai, Shang-Hao Huang

Department of Mechanical Engineering, National Chiao Tung University, Hsinchu 30010, Taiwan, ROC

ARTICLE INFO

Available online 4 September 2013

Keywords:
Moving boundary
Piston cooling
Forced convection
GMRES
PCD preconditioning

ABSTRACT

An enhancement of the back region forced convection heat transfer rates of a reciprocating curved channel with a rib by the ALE method is investigated numerically. In order to avoid damage caused by a huge difference of heat transfer rates between the front and back regions of a reciprocating curved channel, a rib is selected and installed at an appropriate location to enhance the heat transfer rate of the back region. In the ALE method, the generalized minimal residual method preconditioned by the mesh free pressure convection–diffusion in which the pressure terms are arranged in a finite element linearized matrix system is used to solve governing equations. The results show that the heat transfer rate of the back region is indeed enhanced by the installation of the rib at an appropriate location.

1. Introduction

The heat transfer mechanisms of a reciprocating heated object cooled by heat convection modes are very interesting and complicated because a dynamic interaction between the object and cooling fluids is inevitable. Lots of numerical and experimental literature [1–8] then investigated the above subject uninterruptedly for deepening academic research and stretching industrial applications. A reciprocating curved channel well recognized as an operating piston is a kind of the reciprocating heated object and investigated by authors numerically and experimentally [9–13]. Based on detailed analyses of above results, heat transfer rates of the front heated surface where is near the inlet are remarkable because the front heated surface is directly impinged by cooling fluids. Oppositely, heat transfer rates of the back heated surface where is near the outlet are rather inferior since cooling fluids already turn to the outlet before reaching the back region. An apparent difference of heat transfer rates between the front and back regions easily causes thermal damage to occur and should be avoided as much as possible. An issue of enhancing heat transfer rates of the back region to decrease the occurrence of the thermal damage becomes important and urgent.

The work aims to select an appropriate location to install a rib for enhancing heat transfer rates of the back region. The work is classified into a moving boundary problem, and then the Arbitrary Lagrangian and Eulerian (ALE) method is suitable to be adopted as the solution method of this work. The generalized minimal residual method (GMRES) [14] preconditioned by the mesh free pressure convection–diffusion (PCD) [15] in which the pressure terms are arranged in a finite element linearized matrix system is utilized to solve governing equations. The compressed row storage (CRS) [16] matrix format deals with a spare matrix of the PCD to decrease usage of storage memory, as well a distributed memory parallel technique is used to economize computing time. The results that show that the rib installed at the appropriate location can substantially enhance heat transfer rates of the back region that leads to the damage caused by the thermal unbalance between the front and back regions need to be improved.

2. Physical model

A physical model of this work is a two dimensional curved channel which is composed of two vertical channels and a horizontal channel and shown in Fig. 1. The total width and length are w_1 and h_0, respectively, and the width of the channel is w_0. A high and constant temperature T_h is set on the top surface $\overline{BC}$. In order to examine the enhancement of heat transfer rates of the back region, the top surface is evenly divided into three regions of front, middle and back. Cooling fluids of which the temperature and velocity are T_0 and v_0, respectively, via the left vertical channel flow into the curved channel. The other surfaces are adiabatic. Five different locations indicated by dashed lines of ribs evenly distributed on the horizontal channel are used to select an appropriate location to enhance heat transfer rates of the back region. The height and width of the rib are h_2 and w_3, respectively. The interval of ribs is w_2. The region between the $\overline{OP}$ and $\overline{MN}$ is flexible and be elongated from w_0 to $w_0 + l_C$. The magnitude of l_C is the reciprocating amplitude. Therefore, computational grids in this region are extensible. As the horizontal channel moves upward that means the $\overline{MN}$ to be fixed and the $\overline{OP}$ to move upward, and the

☆ Communicated by W.J. Minkowycz.

* Corresponding author at: Department of Mechanical Engineering, National Chiao Tung University, 1001 Ta Hsueh Road, Hsinchu 30056, Taiwan.
E-mail address: wsfu@mail.nctu.edu.tw (W.-S. Fu).

0735-1933/$ – see front matter © 2013 Elsevier Ltd. All rights reserved.
http://dx.doi.org/10.1016/j.icheatmasstransfer.2013.08.005

Nomenclature

$A_{b.r.}$	Area of back region $\left(=\frac{w_1}{3}\right)$
b	Right hand side vector of N–S equation
B	Discretized coefficient matrix of the pressure differential terms
BBt	Preconditioning coefficient matrix
c	Dimensionless computational variable of θ
D	Discretized coefficient matrix of the N–S equation
e	Element number in finite element method
e_1	Unit vector of size k
En	Enhancement factor
f	Right hand side vector of Energy equation
f_C	Dimensional reciprocating frequency of the horizontal channel (s^{-1})
F_C	Dimensionless reciprocating frequency of the horizontal channel
F_P	Bilinear quadrilateral convection–diffusion coefficient matrix
$\widehat{H}_k$	Upper Hessenberg matrix
h_0	Dimensional height of the channel (m)
h_1	Dimensional height of the right vertical channel (m)
h_2	Dimensional height of the rib (m)
k	Number of the GMRES iterations
K	Coefficient matrix of the N–S equation
l_C	Dimensional reciprocating amplitude of the horizontal channel (m)
L	Coefficient matrix of the Energy equation
L_C	Dimensionless reciprocating amplitude of the horizontal channel
m	Number of non-linear iterations of the N–S equation
M	Preconditioning operator matrix
M_F	Quadratic quadrilateral convection–diffusion coefficient matrix
M_P	Bilinear quadrilateral mass coefficient matrix
ne	Total numbers of elements in flow field
p	Dimensional pressure (N m^{-2})
P	Dimensionless pressure
P_B	Dimensionless surface-averaged pressure at inlet surface
P_X	Dimensionless pressure at inlet surface
Pr	Prandtl number ($=\upsilon/\alpha$)
p_∞	Dimensional reference pressure (N m^{-2})
r_0	Initial residual vector of the GMRES method
$\bar{r}_k$	Normalized residual vector at k step of the GMRES method
$\widehat{r}_k$	Unorthonormalized residual vector at k step of the GMRES method
Re	Reynolds number ($=v_0 w_0/\upsilon$)
t	Dimensional time (s)
T	Dimensional temperature (K)
T_0	Dimensional reference temperature (K)
T_H	Dimensional high temperature (K)
u, v	Dimensional velocities of $x-$ and $y-$ directions (ms^{-1})
U, V	Dimensionless velocities of X- and Y- directions
v_0	Dimensional velocity of the inlet cooling air (ms^{-1})
v_C	Dimensional reciprocating velocity of the piston (ms^{-1})
V_C	Dimensionless reciprocating velocity of the piston
v_m	Dimensional maximum velocity of the piston (ms^{-1})
V_m	Dimensionless maximum velocity of the piston
$\widehat{v}$	Dimensional mesh velocity in $y-$ direction (ms^{-1})
$\widehat{V}$	Dimensionless mesh velocity in Y- direction
V_η	Dimensionless node velocity of the moving mesh region
w_0	Dimensional width of the channel (m)
w_1	Dimensional length of the horizontal channel (m)
w_2	Dimensional distances between locations of rib installation (m)
w_3	Dimensional width of the rib (m)
x, y	Dimensional Cartesian coordinates (m)
X, Y	Dimensionless Cartesian coordinates
Z	Discretized coefficient matrix of the Energy equation

Greek symbols

υ	Kinematic viscosity ($m^2 s^{-1}$)
α	Thermal diffusivity ($m^2 s^{-1}$)
τ	Dimensionless time
Δτ	Dimensionless time step interval
τ_P	Dimensionless time interval of a periodic cycle
ρ_0	Dimensional density of air (kg m^{-3})
η_i	Vertical position of the node in the moving mesh region
η_0	Vertical total length of the moving mesh region
θ	Dimensionless temperature
φ	Dimensionless computational variables U, V and P
ζ_k	Intermediate vector at k step of the GMRES method

Other

||||	Normalized value
[]	2-dimensional matrix value
{ }	Vector value

maximum moving distance is l_C. Afterward, the $\overline{OP}$ moves downward and returns to the original location. The moving velocity is v_C expressed in terms of $v_C = v_m \sin(2\pi f_C t)$ in which v_m and f_C are the maximum velocity and frequency, respectively. The maximum velocity is equal to $2\pi l_C f_C$. The reciprocating motion of the channel affects behaviors of fluids transiently, thus phenomena become time-dependent and could be classified into a kind of moving boundary problem. For satisfying convergence conditions of computation, the length of the right vertical channel h_1 is long enough and the exit conditions of temperature and velocity are both fully developed. For facilitating the analysis, the assumptions are described as follows:

1. An incompressible laminar flow is adopted.
2. Fluid properties are constant and the effect of the gravity is neglected.
3. A no-slip condition is held on all surfaces. The fluid velocities on moving boundaries is equal to the boundary moving velocities.

Based upon the characteristic scales of w_0, v_0, $\rho_0 v_0^2$ and T_0, the dimensionless variables are defined as follows:

$$\begin{aligned} &X = \frac{x}{w_0}, Y = \frac{y}{w_0}, U = \frac{u}{v_0}, V = \frac{v}{v_0}, P = \frac{p-p_\infty}{\rho_0 v_0^2}, \\ &\theta = \frac{T\text{-}T_0}{T_h\text{-}T_0}, \widehat{V} = \frac{\widehat{v}}{v_0}, V_C = \frac{v_C}{v_0}, F_C = \frac{f_C w_0}{v_0}, \\ &V_m = \frac{v_m}{v_0}, \tau = \frac{t v_0}{w_0}, Re = \frac{v_0 w_0}{\upsilon}, Pr = \frac{\upsilon}{\alpha} \end{aligned} \tag{1}$$

where $\widehat{v}$ is defined as the mesh velocity.

According to the above assumptions and dimensionless variables, the dimensionless ALE governing equations are expressed as the following equations:

Continuity equation

$$\frac{\partial U}{\partial X} + \frac{\partial V}{\partial Y} = 0 \tag{2}$$

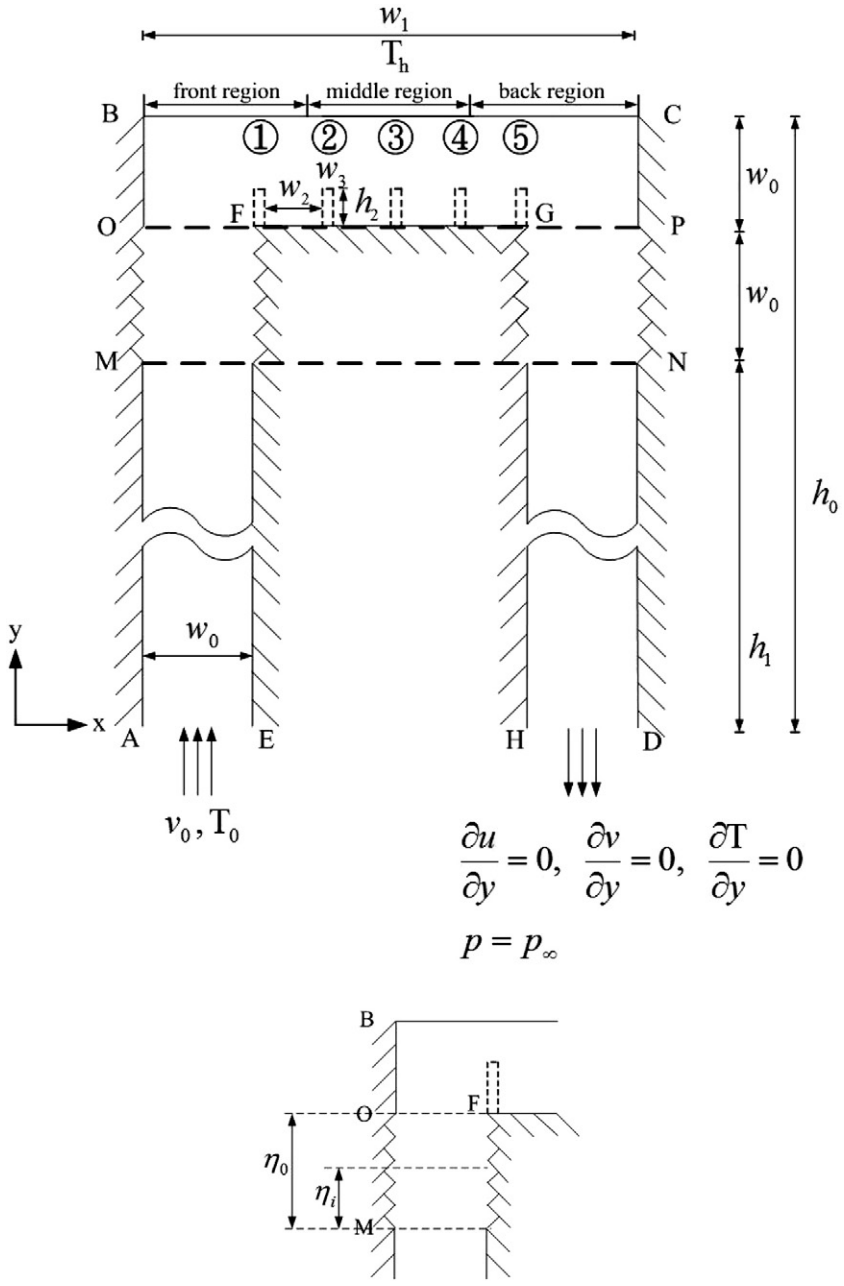

Fig. 1. Physical model.

Momentum equations

$$\frac{\partial U}{\partial \tau}+U\frac{\partial U}{\partial X}+\left(V-\widehat{V}\right)\frac{\partial U}{\partial Y}=-\frac{\partial P}{\partial X}+\frac{1}{Re}\left(\frac{\partial^2 U}{\partial X^2}+\frac{\partial^2 U}{\partial Y^2}\right) \tag{3}$$

$$\frac{\partial V}{\partial \tau}+U\frac{\partial V}{\partial X}+\left(V-\widehat{V}\right)\frac{\partial V}{\partial Y}=-\frac{\partial P}{\partial Y}+\frac{1}{Re}\left(\frac{\partial^2 V}{\partial X^2}+\frac{\partial^2 V}{\partial Y^2}\right) \tag{4}$$

Energy equation

$$\frac{\partial \theta}{\partial \tau}+U\frac{\partial \theta}{\partial X}+\left(V-\widehat{V}\right)\frac{\partial \theta}{\partial Y}=\frac{1}{RePr}\left(\frac{\partial^2 \theta}{\partial X^2}+\frac{\partial^2 \theta}{\partial Y^2}\right). \tag{5}$$

In this study, the curved channel moves upward and downward in the vertical direction only, therefore, the horizontal mesh velocity is absent in the above governing equations. According to the ALE method, the mesh velocities $\widehat{V}$'s are linearly distributed in the region between the $\overline{MN}$ (fixed) and $\overline{OP}$ (movable). In other regions, the mesh velocities $\widehat{V}$'s are equal to 0. Steady state solutions are used as an initial condition before the channel executing reciprocating motion, and the boundary conditions for the physical model are as follows:

At the inlet cross section $\overline{AE}$:

$$U=0, V=1, \frac{\partial P}{\partial Y}=0, \theta=0 \tag{6}$$

At the outlet cross section $\overline{HD}$:

$$\frac{\partial U}{\partial Y}=0, \frac{\partial V}{\partial Y}=0, \frac{\partial \theta}{\partial Y}=0, P=0 \tag{7}$$

Walls between the $\overline{MN}$ and $\overline{OP}$:

$$U = 0, V = \begin{cases} 0 & \tau = 0 \\ V_\eta & \tau > 0 \end{cases}, \frac{\partial P}{\partial X} = 0, \frac{\partial \theta}{\partial X} = 0 \tag{8}$$

Mesh velocities between the $\overline{MN}$ and $\overline{OP}$ are defined as $V_\eta = V_C \times \eta_i/\eta_0$, and are proportional to the distance between the $\overline{MN}$ and $\overline{OP}$.

Vertical walls $\overline{BO}$ and $\overline{CP}$:

$$U = 0, V = \begin{cases} 0 & \tau = 0 \\ V_C & \tau > 0 \end{cases}, \frac{\partial P}{\partial X} = 0, \frac{\partial \theta}{\partial X} = 0 \tag{9}$$

Horizontal wall $\overline{FG}$ and heated wall $\overline{BC}$:

$$\begin{cases} U = 0, V = \begin{cases} 0 & \tau = 0 \\ V_C & \tau > 0 \end{cases}, \frac{\partial P}{\partial Y} = 0, \frac{\partial \theta}{\partial Y} = 0 \\ U = 0, V = \begin{cases} 0 & \tau = 0 \\ V_C & \tau > 0 \end{cases}, \frac{\partial P}{\partial Y} = 0, \theta = 1 \end{cases} \tag{10}$$

Other walls:

$$U = 0, V = 0, \frac{\partial P}{\partial X} = 0, \frac{\partial \theta}{\partial X} = 0. \tag{11}$$

3. Numerical method

The governing equations and boundary conditions are solved by the Galerkin finite element formulation and a backward scheme is adopted to deal with the time terms of the governing equations. The velocity terms are expressed as quadrilateral elements, and eight-node quadratic Lagrangian interpolation is utilized to simplify the non-linear terms in the momentum equations, and pressure terms are expressed as four-node bilinear quadrilateral elements. Then, Eqs. (3) and (4) can be expressed as the following matrix form

$$\sum_1^{ne} [D]^{(e)} \{\varphi\}^{(e)}_{\tau+\Delta\tau} = \sum_1^{ne} ([K_1]^{(e)} + [K_2]^{(e)} + [K_3]^{(e)} + [K_4]^{(e)}) \{\varphi\}^{(e)}_{\tau+\Delta\tau} = \sum_1^{ne} \{b\}^{(e)} \tag{12}$$

where

$$\{\varphi\}^{(e)}_{\tau+\Delta\tau} = \langle U_1, U_2, ..., U_8, V_1, V_2, ..., V_8, P_1, P_2, ..., P_4 \rangle^{m+1}_{\tau+\Delta\tau}. \tag{13}$$

$[K_1]^{(e)}$ includes the (m)th iteration values of U and V at the time $\tau + \Delta\tau$; $[K_2]^{(e)}$ includes a shape function, diffusion terms, $\widehat{V}$ and time differential terms; $[K_3]^{(e)}$ includes the pressure differential terms; $[K_4]^{(e)}$ includes differential terms in the continuity equation; $\{b\}^{(e)}$ includes the known values of U and V at the time τ.

The energy Eq. (5) can be expressed as the following matrix form

$$\sum_1^{ne} [Z]^{(e)} \{c\}^{(e)}_{\tau+\Delta\tau} = \sum_1^{ne} ([L_1]^{(e)} + [L_2]^{(e)}) \{c\}^{(e)}_{\tau+\Delta\tau} = \sum_1^{ne} \{f\}^{(e)} \tag{14}$$

where

$$\{c\}^{(e)}_{\tau+\Delta\tau} = \langle \theta_1, \theta_2, ..., \theta_8 \rangle_{\tau+\Delta\tau}. \tag{15}$$

$[L_1]^{(e)}$ includes the values of U and V at time $\tau + \Delta\tau$; $[L_2]^{(e)}$ includes a shape function, the mesh velocity $\widehat{V}$, diffusion terms, and time differential terms; $\{f\}^{(e)}$ includes the known values of θ at time τ.

In Eq. (12), the Gaussian quadrature procedure is 3×3 quadratic, and conveniently used to execute the numerical integration. The terms within the continuity equation are integrated by bilinear quadrilateral shape functions, while the terms in momentum and energy equations are integrated by quadrilateral shape functions.

The iterative preconditioned GMRES method is applied to solve Eqs. (12) and (14), and the calculation of the initial residual $\{r_0\}$ is expressed as

$$\{r_0\} = \sum_1^{ne} \{b\}^{(e)} - \sum_1^{ne} [D]^{(e)} \{\varphi\}^{(e)}_{\tau+\Delta\tau}. \tag{16}$$

The initial residual is normalized by $\|\{r_0\}\|$.

$$\{\bar{r}_0\} = \frac{\{r_0\}}{\|\{r_0\}\|} \tag{17}$$

An unorthonormalized residual $\{\hat{r}_k\}$ is calculated by the following equation in which $[M]^{-1}$ is an inverted preconditioning operator

$$\{\hat{r}_k\} = \left(\sum_1^{ne} [D]^{(e)} \right) \left([M]^{-1} \{\bar{r}_{k-1}\} \right). \tag{18}$$

The product of multiplication of the inverted preconditioning operator $[M]^{-1}$ and vector $\{\bar{r}_{k-1}\}$ is solved by a direct method of the LU decomposition. The preconditioning operation is used to form the approximate solution.

$$\{\varphi\}^{m+1} = \{\varphi\}^m + [M]^{-1} \left(\left[\left\{ \bar{r}_{1\sim k} \right\} \right] \{\zeta_k\} \right), \quad \varphi = u, v, p \tag{19}$$

where $\{\zeta_k\}$ minimizes the solution of $\left\| \|\{r_0\}\| e_1 - \left[\widehat{H}_k\right] \{\zeta_k\} \right\|$. e_1 is the unit vector of the size k and $[\widehat{H}_k]$ is the upper Hessenberg matrix resulting from the GMRES procedure.

The PCD preconditioning method [15] is applied to solve the momentum equation of Eq. (12), and the operator $[M]$ is expressed as the following form.

$$[M] = \begin{bmatrix} [M_F] & [B] \\ 0 & -[BBt]\,[F_P]^{-1}[M_P] \end{bmatrix} \tag{20}$$

where the $[M_F]$ and $[B]$ are coefficient matrices containing the $\sum_1^{ne} \left([K_1]^{(e)} + [K_2]^{(e)} \right)$ and $\sum_1^{ne} [K_3]^{(e)}$ indicated in Eq. (12), respectively; $[M_P]$ and $[F_P]$ are bilinear quadrilateral integrated mass and convection–diffusion matrices, respectively. As well, the Robin boundary condition [17] is applied to the matrix $[F_P]$; the $[BBt]$ means the multiplication of the $[B]$ with each row divided by corresponding diagonals of the $[M_F]$ and a transposed matrix of the $[B]$.

When the preconditioning operator $[M]$ is used for solving the energy equation, it only contains the $\sum_1^{ne} \left([L_1]^{(e)} + [L_2]^{(e)} \right)$ indicated in Eq. (14).

A brief outline of the solution procedure is described as follows.

1. Determine an optimal mesh distribution and number of the elements and nodes.
2. Solve the values of U, V and P at a steady state and regard them as initial values.

Table 1
Relative length parameters and solid surface mesh divisions of the horizontal channel.

Labels	w_0/w_0	w_1/w_0	w_2/w_0	w_3/w_0	h_2/w_0
Relative length	1	7	1.23	0.04	0.3

3. Determine the time step $\Delta\tau$ and the moving mesh velocities $\hat{V}$ of the computational meshes.
4. Update the coordinates of the nodes and examine the determinant of the Jacobian transformation matrix to ensure the one to one mapping to be satisfied during the Gauss integration.
5. Calculate the corresponding coefficient matrix $[D]^{(e)}$ and preconditioning matrices of $[M_F]$, $[B]$, $[M_P]$, $[F_P]$ and $[BBt]$ with the previous iteration values of the flow field.
6. Solve Eq. (18) and orthonormalize the $\{\bar{r}_k\}$ with previous vectors of the $\{\bar{r}_{1\sim k-1}\}$ by the modified Gram–Schmidt procedure within the GMRES iterations to obtain the $\{\bar{r}_k\}$. The convergent criterion for GMRES iteration is

$$\left\|\frac{\{r_k\}}{\{r_0\}}\right\|<1.0\times10^{-6}. \tag{21}$$

7. Adopt the $\left[\left\{\bar{r}_{1\sim k}\right\}\right]$ obtained from step (6) to solve Eq. (19) and obtain the approximate solution $\{\varphi\}^{m+1}$, where φ = U, V and P for Eq. (12) and $\varphi = \theta$ for Eq. (14).
8. Repeat steps (5)–(7) until the following criteria for momentum equations are satisfied

$$\left|\frac{\varphi^{m+1}-\varphi^{m}}{\varphi^{m}}\right|<1.0\times10^{-3}. \tag{22}$$

9. With converged flow field values of U, V and P, calculate the coefficient matrix $[Z]^{(e)}$ and regard it as the preconditioning matrix. Apply steps (6) and (7) repeatedly until the relative residual reaches the criterion defined by Eq. (21).
10. Continue the next time step calculation until periodic solutions are attained.

4. Results and discussion

Related lengths used in this work are tabulated in Table 1. The respective distributions of streamlines and isothermal lines of different locations (cases 1-5) of the rib and without the rib (case 0) are indicated

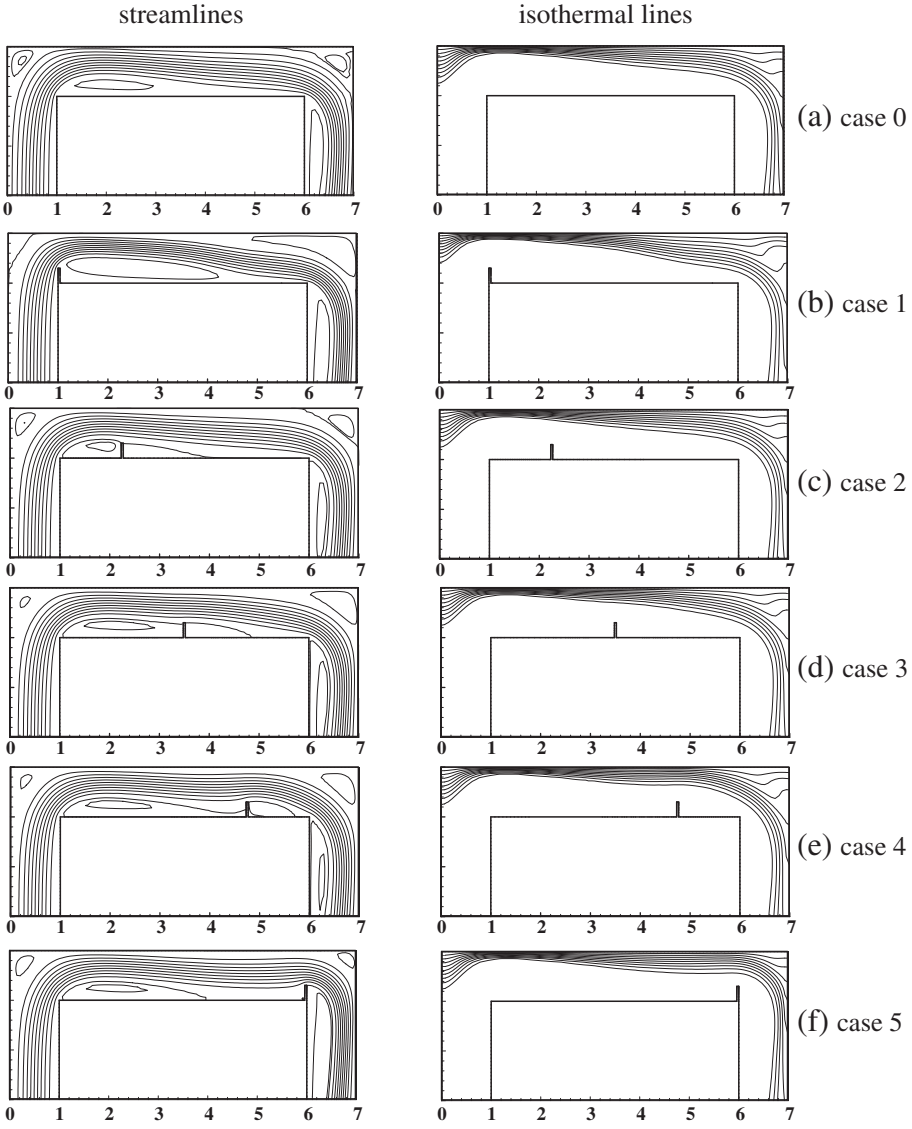

Fig. 2. Comparisons of distributions of streamlines and isothermal lines for cases 0-5 at a stationary situation under Re = 200.

in Fig. 2. The results of the case 0 were indicated in the previous study [9]. Distributions of streamlines and isothermal lines are deeply affected by the location of the rib. In the case 1, the impingement of cooling fluids on the front region is more apparent than the other cases. In the case 5, due to the impediment of the rib cooling fluids are compulsively postponed to flow into the right vertical channel that causes cooling fluids to flow through a large area of the back region relative to the other cases. This phenomenon is able to enhance heat transfer rates of the back region.

Comparisons of local Nusselt numbers of the back region of different locations of the rib with that of without a rib case are indicated in Fig. 3, respectively. The definition of the local Nusselt number Nu_X of the back region and enhancement factor En of the back region are expressed as follows, respectively,

$$Nu_X = -\frac{\partial\theta}{\partial Y} \tag{23}$$

$$\overline{Nu} = \frac{1}{A_{b.r.}}\int_{A_{b.r.}} Nu_X dX \tag{24}$$

$$En = \frac{\overline{Nu}_{case\ 1\text{–}5}}{\overline{Nu}_{case\ 0}}. \tag{25}$$

The purpose of this work is to improve heat transfer rates of the back region of the curved channel. According to the results shown in Fig. 3, the improvement of heat transfer rates of the back region is remarkably achieved by the case 5. Then the case 5 is selected to investigate the improvement of heat transfer rates of the back region as the curved channel is subject to reciprocating motions.

Local Nusselt numbers of cases 0 and 5 at different stages of a periodic cycle are separately revealed in Fig. 4. At each stage the improvements of heat transfer rates of the back region are always achieved.

The respective magnitudes of the enhancement factor under the situations composing different Reynolds numbers, frequencies and amplitudes are tabulated in Table 2. In each situation, the aim of this work is achieved. The maximum magnitude of the enhancement is about 50%.

5. Conclusions

A numerical work of investigation of the enhancement of forced convection heat transfer rates of a reciprocating curved channel with a rib is

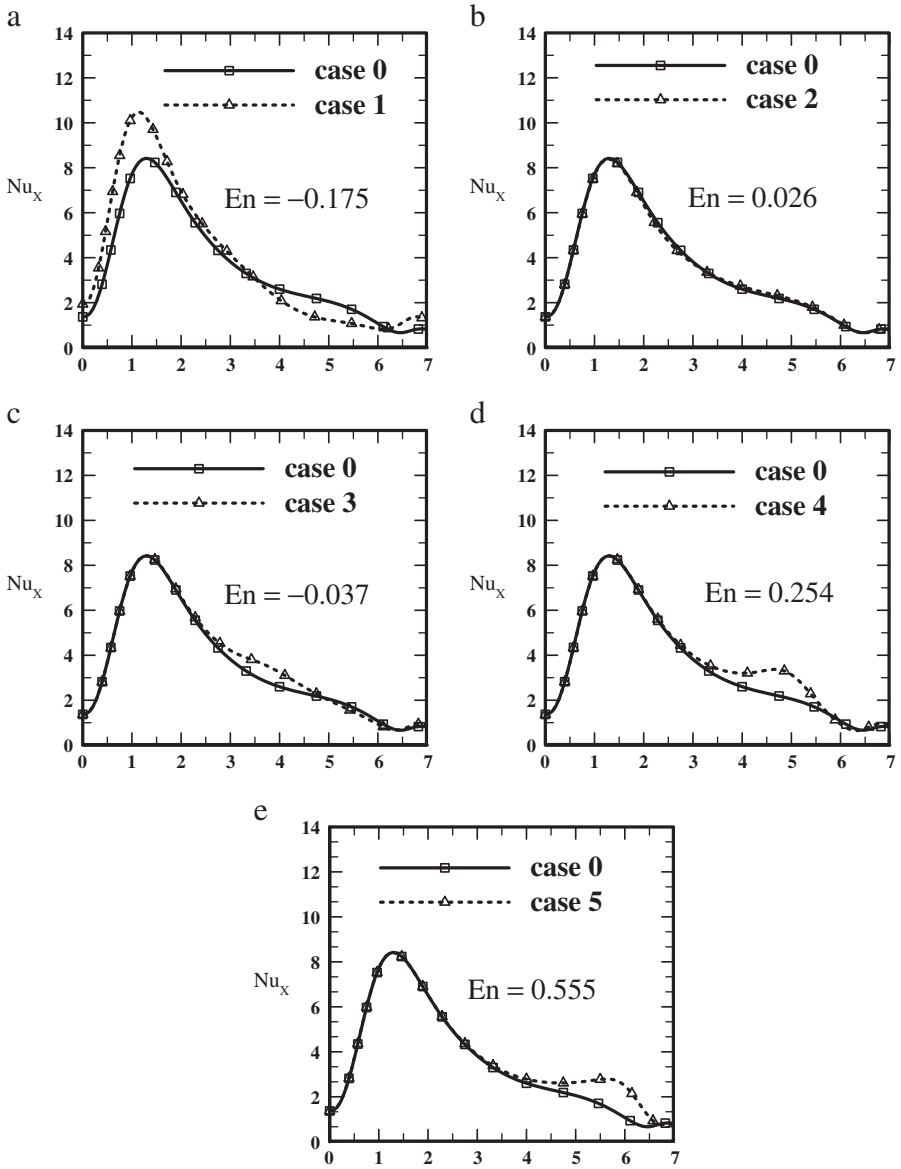

Fig. 3. Comparisons of Nusselt number distributions of the case 0 with cases 1-5 at a stationary situation under Re = 200.

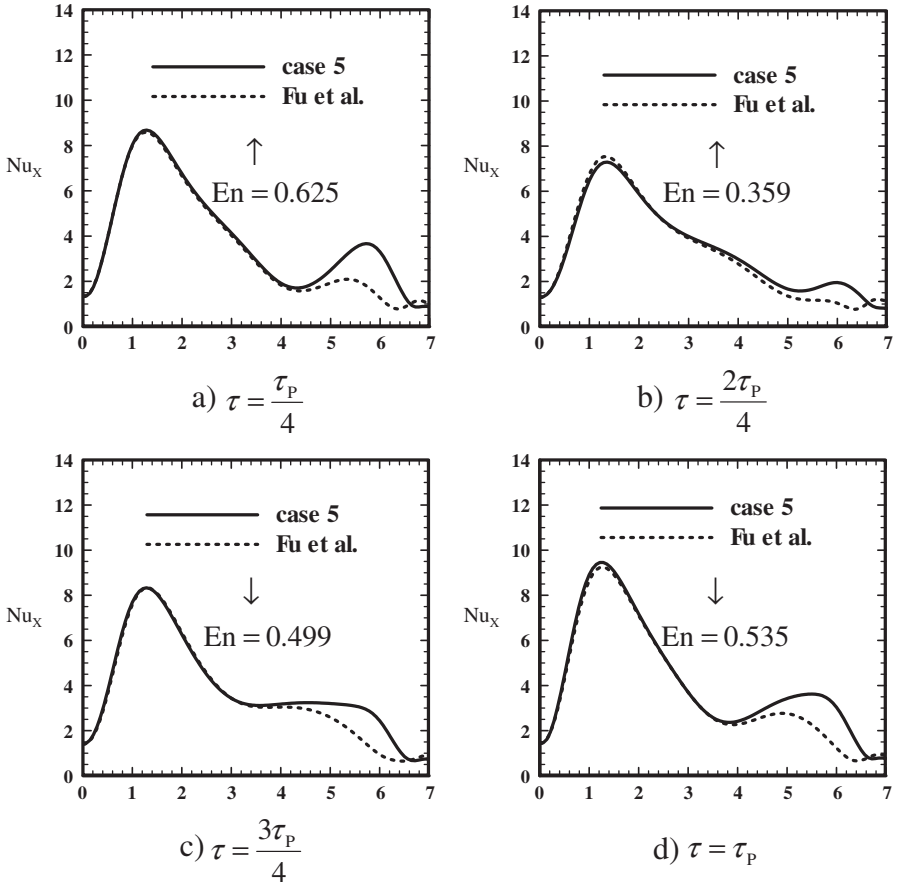

Fig. 4. Comparisons of local Nusselt number distributions of the case 0 with case 5 at Re = 200, L_C = 0.25 and F_C = 0.1 situation.

studied. An appropriate location which is the location 5 is selected from five different locations to achieve the heat transfer rate of the back region of the curved channel. The following conclusions are drawn.

(1) The location 5 of the rib is effective to guide cooling fluids to flow through a large surface of the back region, and it is the main reason to enhance heat transfer rates of the back region.
(2) Under situations of different Reynolds numbers, frequencies and amplitudes, the magnitudes of the enhancements of the heat transfer rate of the back region are remarkable. The maximum magnitude is about 50%. The decrement of the difference of heat transfer rates of the front and back regions is achieved by the rib installed at the location 5.

References

[1] P.P. Grassmann, M. Tuma, Applications of the electrolytic method-II. Mass transfer within a tube for steady, oscillating and pulsating flows, Int. J. Heat Mass Transfer 22 (1979) 799–804.
[2] A.T. Patera, B.B. Mikic, Exploiting hydrodynamic instabilities resonant heat transfer enhancement, Int. J. Heat Mass Transfer 29 (8) (1986) 1127–1138.
[3] S.Y. Kim, B.H. Kang, A.E. Hyun, Heat transfer in the thermally developing region of a pulsating channel flow, Int. J. Heat Mass Transfer 36 (17) (1993) 1257–1266.
[4] T. Nishimura, N. Kojima, Mass transfer enhancement in a symmetric sinusoidal wavy-walled channel for pulsatile flow, Int. J. Heat Mass Transfer 38 (9) (1995) 1719–1731.
[5] C.P. Chiu, Y.S. Kuo, Study of turbulent heat transfer in reciprocating engine using as algebraic grid generation technique, Numer. Heat Transfer, Part A 27 (1995) 255–271.
[6] C.H. Cheng, C.K. Hung, Numerical predictions of flow thermal fields in a reciprocating piston–cylinder assembly, Numer. Heat Transfer, Part A 38 (2000) 397–421.

Table 2
Combinations of computational parameters, results of this study and Fu et al. [1] under stationary and reciprocating motions.

Case	Rib position	Re	L_C	F_C	V_m	Back region $\overline{Nu}$ Fu et al.	Back region $\overline{Nu}$ Present study	En
0	No rib	200	–	–	–	0.6725	0.6725	0
1	①	200	–	–	–	0.6725	0.5545	–0.175
2	②	200	–	–	–	0.6725	0.6906	0.026
3	③	200	–	–	–	0.6725	0.6473	–0.037
4	④	200	–	–	–	0.6725	0.8435	0.254
5	⑤	200	–	–	–	0.6725	1.0463	0.555
6	⑤	200	0.25	0.1	0.157	1.4541	2.2061	0.517
7	⑤	200	0.25	0.2	0.314	2.0708	2.7167	0.312
8	⑤	200	0.25	0.4	0.628	1.9385	2.8439	0.467
9	⑤	200	0.5	0.1	0.314	1.7325	2.6038	0.503
10	⑤	200	1.0	0.1	0.628	2.5185	3.2839	0.304
11	⑤	500	0.25	0.1	0.157	2.6502	3.7749	0.424
12	⑤	750	0.25	0.1	0.157	3.9736	4.3305	0.089

[7] S.W. Chang, L.M. Su, W.D. Morris, T.M. Liou, Heat transfer in a smooth-walled reciprocating anti-gravity open thermosyphon, Int. J. Heat Mass Transfer 42 (2003) 1089–1103.
[8] S.W. Chang, L.M. Su, Heat transfer in a reciprocating duct fitted with transverse ribs, Exp. Heat Transfer 12 (1999) 95–115.
[9] W.S. Fu, S.H. Lian, L.Y. Hao, An investigation of heat transfer of a reciprocating piston, Int. J. Heat Mass Transfer 49 (2006) 4360–4371.
[10] W.S. Fu, C.P. Huang, Effects of a vibrational heat surface on natural convection in a vertical channel flow, Int. J. Heat Mass Transfer 49 (2006) 1340–1349.
[11] W.S. Fu, S.H. Lian, Y.C. Lai, A mixed convection in a reciprocating shape channel with opposite direction of gravity and inlet cooling fluids, Int. J. Heat Mass Transfer 45 (2009) 679–692.
[12] W.S. Fu, S.H. Lian, C.L. Lin, C.L. Tang, An experimental investigation of a mixed convection in a ⊔ shape channel subject to a reciprocating motion, Int. J. Heat Mass Transfer 52 (2009) 3613–3627.
[13] W.S. Fu, S.H. Lian, Y.C. Lai, An investigation mixed convection in a ⊔ shape channel moving with a reciprocating motion, Int. J. Heat Mass Transfer 36 (9) (2009) 921–924.
[14] Y. Saad, M. Schultz, GMRES: a generalized minimum residual algorithm for solving nonsymmetric linear systems, SIAM J. Sci. Stat. Comput. 7 (1986) 856–869.
[15] H.C. Elman, D.J. Silvester, A.J. Wathen, Finite Elements and Fast Iterative Solvers, Oxford University Press, Oxford, 2005.
[16] Y. Saad, Iterative Methods For Sparse Linear Systems, 2nd edition SIAM, 2003.
[17] H.C. Elman, R. Tuminaro, Boundary conditions in approximate commutator preconditioners for the Navier–Stokes equations, ETNA 35 (2009) 257–280.